Quantum and All-Atom Molecular Dynamics Simulations of Protonation and Divalent Ion Binding to Phosphatidylinositol 4,5-Bisphosphate (PIP$_2$)

David R. Slochower[1], Peter J. Huwe[1], Ravi Radhakrishnan[1,2], and Paul A. Janmey[1,3,]*

[1]Graduate Group in Biochemistry and Molecular Biophysics, Perelman School of Medicine, [2]Department of Bioengineering, School of Engineering and Applied Sciences, [3]Department of Physiology, Perelman School of Medicine, University of Pennsylvania, Philadelphia, PA 19104,

[*]Correspondence addressed to: Paul A. Janmey, 1010 Vagelos Laboratories, 3340 Smith Walk, University of Pennsylvania, Philadelphia, PA 19104, Tel: 215-300-9528, E-mail: janmey@mail.med.upenn.edu

Supporting Information

Using the Gaussian '09 program, the molecular geometry of PIP_2 was obtained using the

Hartree-Fock scheme in conjunction with the 6-31+G(d) basis set. The initial structure

contained a proton placed equidistant between oxygen atoms from the 4-phosphate and 5-

phosphate groups. The final Z-matrix is as follows:

```
c
c      1 cc2
c      2 cc3        1 ccc3
c      3 cc4        2 ccc4         1 dih4
c      4 cc5        3 ccc5         2 dih5
c      5 cc6        4 ccc6         3 dih6
o      2 oc7        3 occ7         4 dih7
p      7 po8        2 poc8         3 dih8
o      8 op9        7 opo9         2 dih9
c      9 co10       8 cop10        7 dih10
c     10 cc11       9 cco11        8 dih11
c     11 cc12      10 ccc12        9 dih12
o     12 oc13      11 occ13       10 dih13
c     13 co14      12 coc14       11 dih14
o     14 oc15      13 oco15       12 dih15
o      3 oc16       2 occ16        7 dih16
o      4 oc17       3 occ17        2 dih17
o      5 oc18       4 occ18        3 dih18
p     18 po19       5 poc19        4 dih19
o     19 op20      18 opo20        5 dih20
o      6 oc21       5 occ21       18 dih21
p     21 po22       6 poc22        5 dih22
o     22 op23      21 opo23        6 dih23
o      1 oc24       2 occ24        7 dih24
o      8 op25       7 opo25        2 dih25
o      8 op26       7 opo26        2 dih26
o     19 op27      18 opo27        5 dih27
o     19 op28      18 opo28        5 dih28
o     22 op29      21 opo29        6 dih29
o     22 op30      21 opo30        6 dih30
o     11 oc31      10 occ31        9 dih31
c     31 co32      11 coc32       10 dih32
c     32 cc33      31 cco33       11 dih33
o     32 oc34      31 oco34       11 dih34
c     14 cc35      13 cco35       12 dih35
h     16 ho36       3 hoc36        2 dih36
h     17 ho37       4 hoc37        3 dih37
h     24 ho38       1 hoc38        2 dih38
h      2 hc39       7 hco39        8 dih39
h      3 hc40       2 hcc40        7 dih40
h      4 hc41       3 hcc41        2 dih41
h      5 hc42      18 hco42       19 dih42
h      6 hc43      21 hco43       22 dih43
h      1 hc44       2 hcc44        7 dih44
h     33 hc45      32 hcc45       31 dih45
h     35 hc46      14 hcc46       13 dih46
h     29 ho47      22 hop47       21 dih47
h     11 hc48      31 hco48       32 dih48
h     33 hc49      32 hcc49       31 dih49
h     33 hc50      32 hcc50       31 dih50
h     35 hc51      14 hcc51       13 dih51
```

```
h   35 hc52        14 hcc52        13 dih52
h   10 hc53        11 hcc53        31 dih53
h   10 hc54        11 hcc54        31 dih54
h   12 hc55        11 hcc55        31 dih55
h   12 hc56        11 hcc56        31 dih56

cc2          1.526344
cc3          1.525584
ccc3         110.464
cc4          1.534422
ccc4         107.977
dih4         -63.226
cc5          1.536272
ccc5         109.996
dih5          65.784
cc6          1.550422
ccc6         112.130
dih6         -54.297
oc7          1.430472
occ7         114.252
dih7         178.785
po8          1.609872
poc8         129.570
dih8         -76.014
op9          1.654558
opo9         100.649
dih9          89.510
co10         1.390493
cop10        118.339
dih10         56.942
cc11         1.525172
cco11        108.169
dih11        -175.973
cc12         1.516607
ccc12        112.077
dih12         53.050
oc13         1.444620
occ13        109.903
dih13        169.421
co14         1.307801
coc14        121.324
dih14         88.633
oc15         1.194599
oco15        126.101
dih15          1.910
oc16         1.415805
occ16        111.903
dih16        -54.700
oc17         1.396342
occ17        108.994
dih17        -171.724
oc18         1.397510
occ18        116.117
dih18        178.192
po19         1.724291
poc19        127.832
dih19         30.224
op20         1.508970
opo20        104.741
dih20         50.797
oc21         1.424589
occ21        112.141
dih21        -64.455
po22         1.622718
poc22        126.247
dih22        -43.036
op23         1.496990
opo23        109.001
dih23        -30.862
oc24         1.418164
occ24        109.016
```

```
dih24        -63.339
op25          1.484818
opo25       106.531
dih25       -159.329
op26          1.474582
opo26       112.354
dih26        -22.804
op27          1.504387
opo27       102.301
dih27       173.149
op28          1.529475
opo28       102.611
dih28        -68.029
op29          1.621747
opo29       100.814
dih29         84.774
op30          1.485743
opo30       108.720
dih30       -162.053
oc31          1.445320
occ31       104.664
dih31       170.387
co32          1.300480
coc32       123.522
dih32       142.520
cc33          1.510033
cco33       110.400
dih33       176.609
oc34          1.200221
oco34       126.449
dih34         -3.727
cc35          1.510545
cco35       110.753
dih35       -177.884
ho36          0.955083
hoc36       111.918
dih36        -68.963
ho37          0.977482
hoc37       105.034
dih37       170.673
ho38          0.948667
hoc38       105.953
dih38         52.346
hc39          1.082596
hco39       108.137
dih39         45.153
hc40          1.082127
hcc40       109.459
dih40         61.497
hc41          1.086439
hcc41       107.608
dih41        -53.191
hc42          1.080006
hco42       104.771
dih42       145.460
hc43          1.080634
hco43       105.331
dih43       -159.036
hc44          1.080878
hcc44       107.794
dih44         54.135
hc45          1.083874
hcc45       109.720
dih45         56.197
hc46          1.083719
hcc46       110.223
dih46        -49.020
ho47          0.961524
hop47       112.864
dih47        -26.260
hc48          1.079439
```

```
hco48        108.416
dih48         22.809
hc49         1.084019
hcc49        109.203
dih49        -61.054
hc50         1.082332
hcc50        110.002
dih50        177.802
hc51         1.082120
hcc51        109.751
dih51       -170.839
hc52         1.084700
hcc52        108.552
dih52         69.339
hc53         1.086291
hcc53        109.176
dih53        -68.761
hc54         1.081245
hcc54        108.631
dih54         49.990
hc55         1.075921
hcc55        110.080
dih55        175.558
hc56         1.077606
hcc56        111.112
dih56        -62.016
```
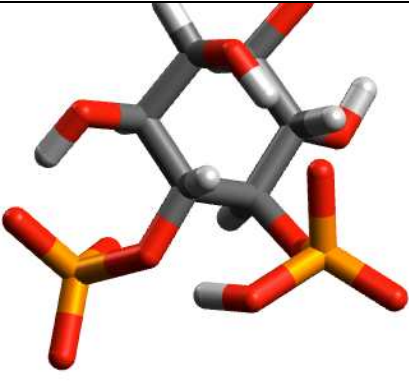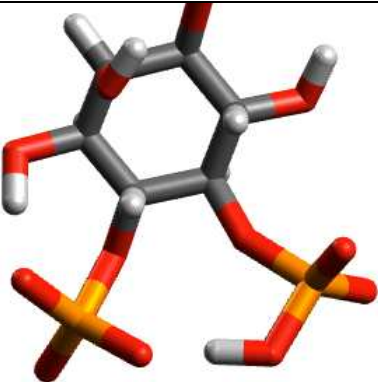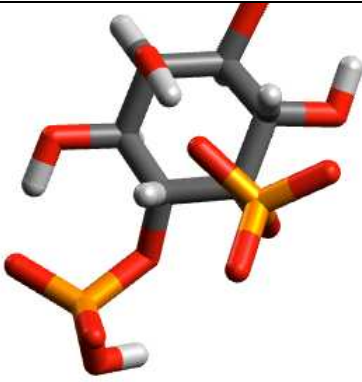
Proton on 5-phosphate	Proton shared between 4 and 5	Proton on 4-phosphate
+15.4 kcal/mol	0 kcal/mol	+22.0 kcal/mol

Figure S1. Relative energies of protonation isomers. The relative stabilities of protonated PIP$_2$ isomers were computed with Gaussian 09 at the HF/3-21G level of theory with implicit water solvent using a Polarizable Continuum Model[1-3]. Relaxed dihedral potential energy scans were used to identify energetic minima among isomers. In the lowest energy structure (middle panel), the proton is shared between the 4 and 5-phosphates. The distances from the proton to the 5 and 4-phosphate oxygens are 1.11 Å and 1.30 Å, respectively. This shared state is 15.4 kcal/mol and 22.0 kcal/mol more stable than localization to the 5-phosphate (left panel) or the 4-phosphate (right panel), respectively.

Our results are obtained from all-atom molecular dynamics simulations of membrane bilayers of 800 total lipids containing PIP2 in the presence of phosphatidylcholine (PC), phosphatidylserine (PS), phosphatidylethanolamine (PE), and cholesterol with 150 mM NaCl in a solvent box containing approximately 80,000 waters. The outer leaflet contains 300 POPC [3-palmitoyl-2-oleoyl-D-glycero-1-phosphatidylcholine] molecules and 100 cholesterol molecules. The inner leaflet contains 200 DOPE [2,3-dioleyl-D-glycero-1-phosphatidylethanolamine] molecules, 100 cholesterol molecules, 60 DOPS [2,3-dioleyl-D-glycero-1-phosphatidylserine] molecules, 40 SA-PIP2 [1-stearoyl-2-arachadonyl-*sn*-glycero-1-phosphatidylinositol-4,5-bisphosphate] molecules. The lipids were packed at approximately 65 $Å^2$ per lipid and randomly seeded with PIP_2 typically about 10% of the total lipids on one leaflet. The system was equilibrated for 10 ns before the production run, for which the analysis is presented below. We used the CHARMM36 lipid forcefield in the GROMACS simulation package[4-7] to prepare membrane bilayers in an NPT ensemble and have simulated for 31 ns so far, using a 2 fs timestep. Pressure is maintained using the Parrinello-Rahman barostat[8,9], coupled independently (semi-isotropic) in directions normal and perpendicular to the bilayer with a time constant of 2.0 ps and a pressure of 1 bar. Electrostatics are treated with the particle mesh Ewald (PME)[10] method with cubic periodic boundaries, using a real space cutoff of 1.2 nm and a Fourier grid spacing of 0.16 nm with cubic interpolation. Temperature coupling is accomplished using the thermostat due to Bussi[11], in which velocity is rescaled with a stochastic term. These simulations employ the CHARMM-specific TIP3P (i.e., TIPS3P) water model (with van der Waals interactions on the water hydrogen atoms) and van der Waals interactions which are smoothly switched off between 0.8 and 1.2 nm[12].

Histograms were computed (Figure S2) for the QM/MM simulations presented in the main text (a single PIP2 molecule in a water sphere) and for each lipid every 20 frames of the classical all-atom trajectory. The head-tail angle was measured as described in the main text. Our QM/MM and classical bilayer simulation results quantitatively agree with each other, but disagree if we employ the parameters of Lupyan, et al.
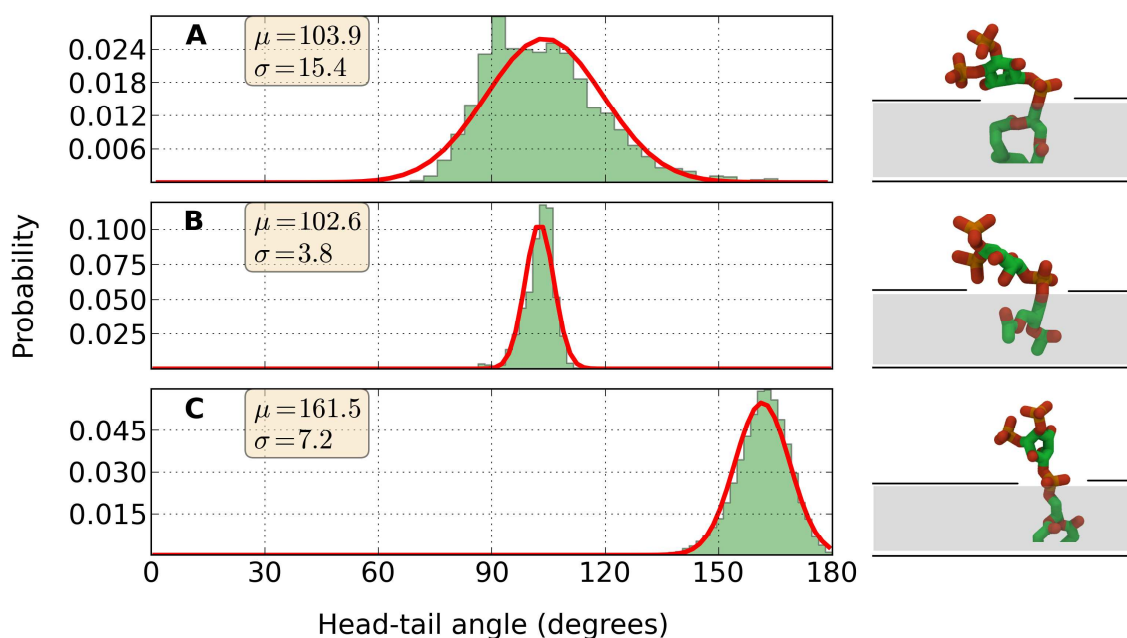

Figure S2. **A**. The probability distribution for 80 PIP_2 lipids in one leaflet of a bilayer also containing phosphatidylserine, phosphatidylethanolamine, and cholesterol. The histogram was averaged over each lipid and every 20 frames of the all-atom simulation for 15 ns using CHARMM36 lipid parameters. The mean head-tail angle is 104 degrees. **B.** The probability distribution of the angle between the PIP_2 headgroup and the PIP_2 acyl chains as measured from an isolated PIP_2 molecule in a water sphere over 10 ps of a QM/MM simulation. Sodium ions were present for charge neutrality but fixed to be ~10 Å away from the PIP_2. The mean head-tail angle is 103 degrees. **C.** The probability distribution from a simulation of a bilayer containing pure PIP_2 using the same system parameters as panel A, but with the parameters of Lupyan, et al. used instead of the CHARMM36 lipid parameters[13]. The average head-tail angle is 162 degrees.

We computed the average PIP$_2$ molecular area in membrane bilayer systems to compare with the QM/MM results presented in the main text. Since there was only a single molecule in the QM/MM simulations, we used the separation of the phosphate groups as a proxy for molecular area. To calculate the molecular area in the bilayer simulations, we projected the center of gravity of each lipid onto a plane and created a Delaunay triangulation. We summed the area created by forming a polygon from the bisector of each line meeting a vertex corresponding to PIP$_2$. There are subtleties in defining the average molecular area of lipids in a heterogeneous bilayer simulation and these methods are still evolving.

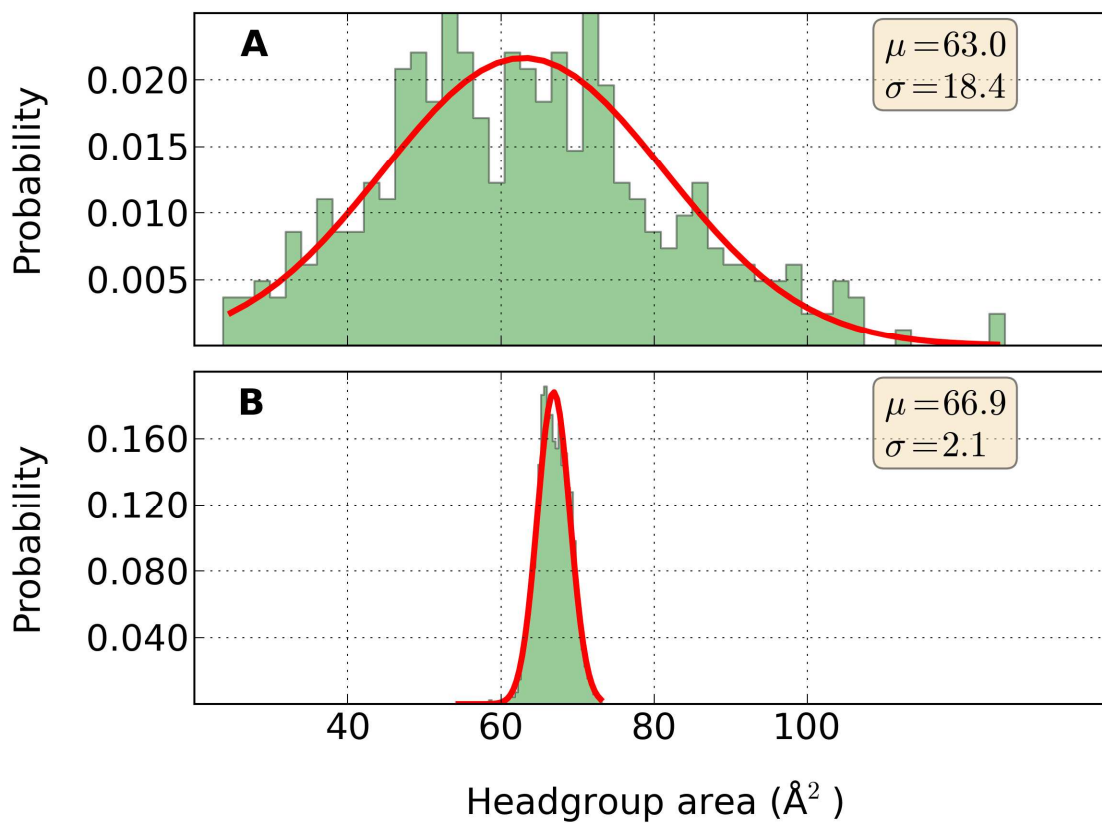Figure S3. **A**. The probability distribution for 80 PIP$_2$ lipids in a bilayer also containing phosphatidylcholine, phosphatidylserine, and phosphatidylethanolamine. **B**. The probability distribution of the approximate molecular area of PIP$_2$ as measured from an isolated PIP$_2$ molecule in a water sphere over 10 ps of a QM/MM simulation. Sodium were present for charge neutrality but fixed to be ~10 Å away from the PIP$_2$.
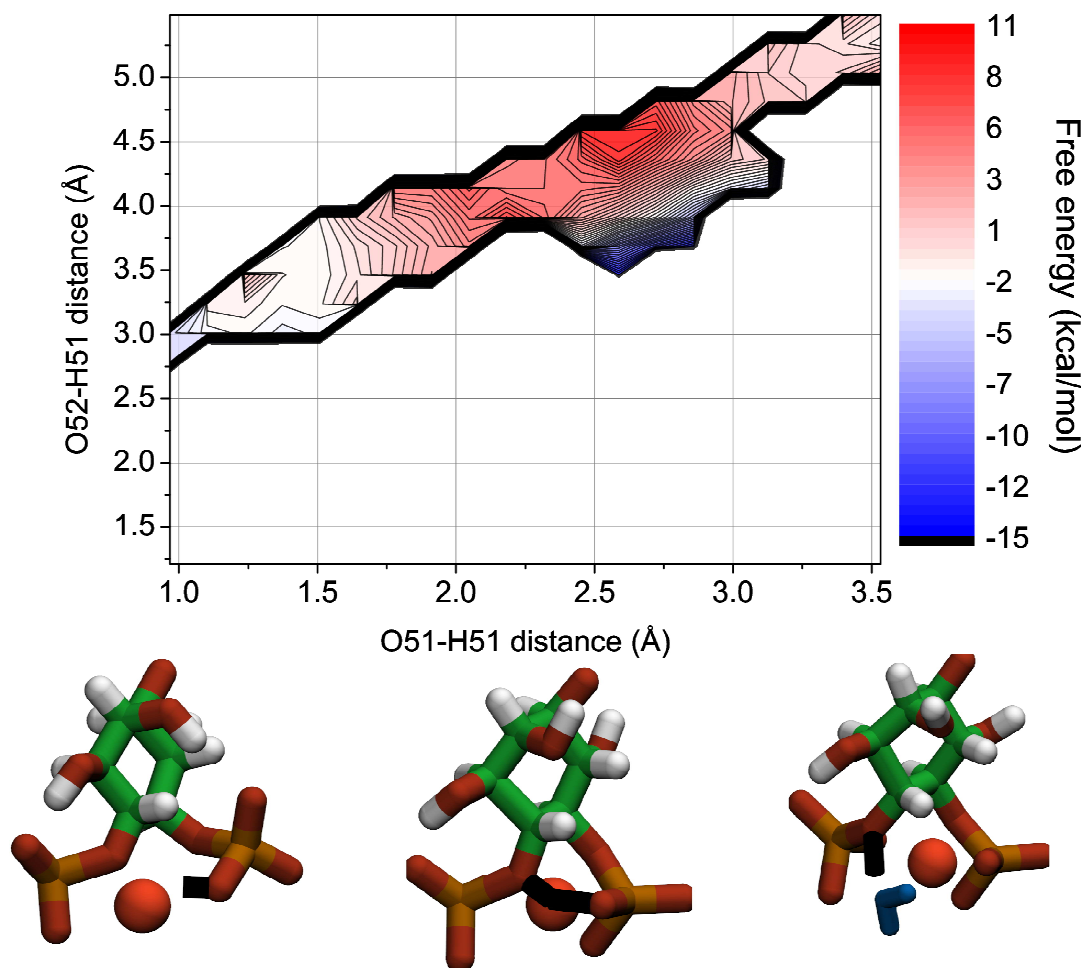
Figure S4. The free energy landscape for dissociating a proton from the 5-phosphate group of PIP$_2$. Full deprotonation in the presence of magnesium has not been achieved. Insets show magnesium (in red) between the two phosphomonoester groups of PIP$_2$ and the proton to be dissociated in black. The initial state of the QM/MM 2D umbrella sampling is on the left, with proton H51 bound to oxygen O51. The inset in the middle corresponds to the energy well on the contour plot (blue), where proton H51 is shared between oxygen O51 and oxygen O4P. The inset on the right corresponds to the final window of the trajectory, where proton H51 is shared between oxygen O4P of PIP$_2$ and a QM water (in blue).

It is possible to calculate pKa values from the free energy plots presented in the main text. To do this, we consider the canonical definition of the association constant, K_a, between a ligand, L, and its binding partner, R, in terms of the ratio of the probabilities of being not bound or bound. In this case, we take the ligand to be a proton and its binding partner to be a PIP_2 molecule. So we write,

$$K_a = \frac{1}{[L]} \times \frac{\mathcal{P}_{bound}}{\mathcal{P}_{unbound}}$$

where $\mathcal{P}_{bound}$ and $\mathcal{P}_{unbound}$ can be determined by integrating over the degrees of freedom and the potentials of mean force. pKa is related to K using the following relationship:

$$pKa = \log_{10}\left| K_a \times \frac{1}{1661 \text{Å}^3} \right|$$ using the standard concentration of 1 mol/liter = 1/1661 Å^3.

We can perform the pKa calculation in two ways. In the first method, we integrate the bound state until $r = r^\star$ which is the point where the proton leaves the domain of influence of the oxygen to which it was originally bound. This is judged by viewing the simulation trajectories and looking at the minima of the potentials of mean force. The unbound state is integrated from $r = r^\star$ until the final point in the energy landscape.

In the second method, we integrate the bound state until $r = r^\star$ as before. To evaluate the unbound state, we integrate from $r = r^\star$ until the next metastable minimum at $r = r^{\star\star}$. In this technique, events that we categorize as dissociation, such as proton transfer to other atoms on PIP_2, may not correspond to dissociation events judged from experiments.

Values for $r^\star$ and $r^{\star\star}$ and the results of these calculations are shown in Figure S5. Error

bars in the pKa calculation represent the outcome of changing the value of $r^\star$ by 0.25 Å or approximately the width of a well in the potential of mean force.

We stress that the absolute value of these numbers should not be compared to the results of experiments due to the approximations necessary in obtaining absolute free energy curves from the potentials of mean force calculated along a single reaction coordinate. Kooijman et al. calculate the pKa of PIP$_2$ in lipid vesicles, which is different from our case in several respects (e.g., the effect of a negative surface charge density of the vesicle membrane) so a direct comparison is not strictly valid[14]. Moreover, the pKa values reported by Kooijman et al. correspond to PI(3,5)P$_2$ and PI(3,4,5)P$_2$ which could have different ionization properties due to the positioning of the phosphate groups. In fact, for PI(4,5)P$_2$, Kooijman et al. note that a biphasic pH-dependent ionization behavior that cannot be explained by a Henderson-Hasselbach equation was obtained. Our calculations are consistent with this; our free energy landscape does not simply represent two states (bound or unbound) but displays intermediate metastable states. These states correspond to sharing of the proton between the vicinal phosphomonoester groups. Hence, our pKa should be regarded as an apparent pKa for proton transfer from the host oxygen (O51 in the main text) to the next energetically favorable state (rather than a free unbound state).

The subtleties caused by a complex (rugged) free energy landscape and non-independence of proton binding to vicinal sites cause problems in defining an absolute pKa; moreover, the apparent pKa is subject to the definitions of vicinal binding sites as metastable states (or our choice of $r^{\star\star}$). Another complexity is a computational one. In the QM/MM potentials of mean force, the energy landscape is only accurate for short

excursions from the initial bound state along the reaction coordinate. For longer

excursions, the wave functions from the QM region are spread over larger volumes

causing an imbalance in basis set superposition. Also for these large distances along the

reaction coordinate, close interaction between classical charges and the QM wave

function become significant.

In general, we find that the pKa for protonation of PIP_2 in the presence of calcium is the

smallest, implying strong dissociation of the proton. The pKa in the presence of

magnesium is similar to that of a pure water environment, where we find protonation of

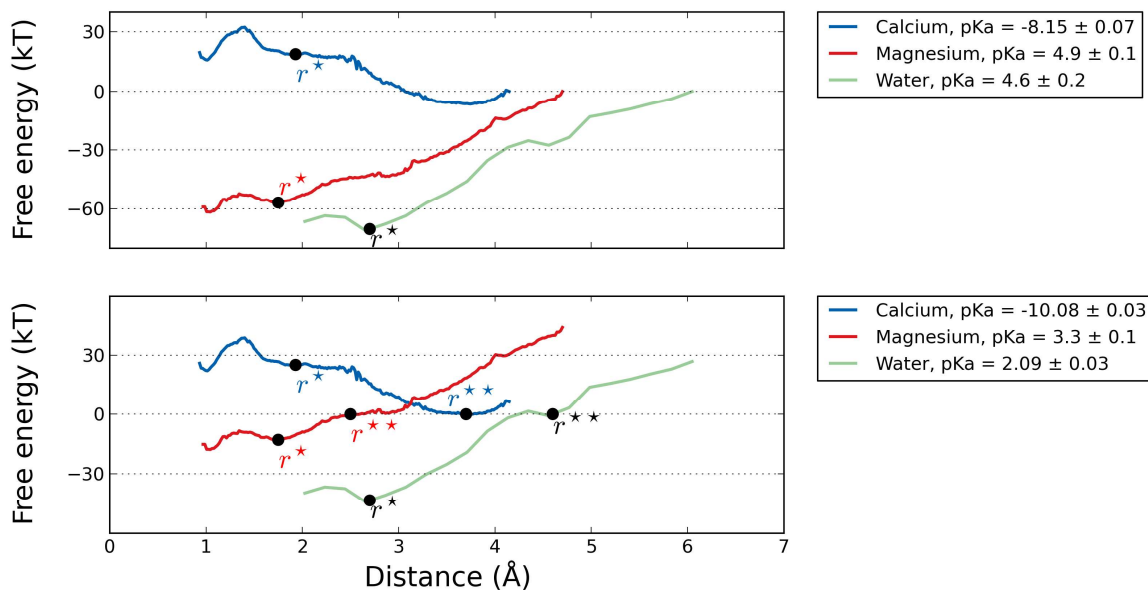PIP_2 on the 5-phosphate group to be the most stable conformation.

Figure S5. The potentials of mean force for proton dissociation from PIP_2 in a water sphere with either calcium, magnesium, or pure water. In the latter case, sodium ions are present for charge neutrality but confined ~10 Å away from the PIP_2.

(1) Miertuš, S.; Scrocco, E.; Tomasi, J. Electrostatic Interaction of a Solute with a Continuum. A Direct Utilization of Ab Initio Molecular Potentials for the Prevision of Solvent Effects *Chem. Phys.* **1981**, *55*, 117–129.

(2) Pascual-ahuir, J. L.; Silla, E.; Tu on, I. GEPOL: an Improved Description of Molecular Surfaces. III. a New Algorithm for the Computation of a Solvent-Excluding Surface *J. Comp. Chem.* **1994**, *15*, 1127–1138.

(3) Tomasi, J.; Mennucci, B.; Cammi, R. Quantum Mechanical Continuum Solvation Models. *Chem. Rev.* **2005**, *105*, 2999–3093.

(4) Van Der Spoel, D.; Lindahl, E.; Hess, B.; Groenhof, G.; Mark, A. E.; Berendsen, H. J. C. GROMACS: Fast, Flexible, and Free *J. Comp. Chem.* **2005**, *26*, 1701–1718.

(5) Bjelkmar, P.; Larsson, P.; Cuendet, M. A.; Hess, B.; Lindahl, E. Implementation of the CHARMM Force Field in GROMACS: Analysis of Protein Stability Effects From Correction Maps, Virtual Interaction Sites, and Water Models *J. Chem. Theo. Comput.* **2010**, *6*, 459–466.

(6) Klauda, J. B.; Monje, V.; Kim, T.; Im, W. Improving the CHARMM Force Field for Polyunsaturated Fatty Acid Chains. *J. Phys. Chem. B* **2012**, *116*, 9424–9431.

(7) Klauda, J. B.; Venable, R. M.; Freites, J. A.; O'Connor, J. W.; Tobias, D. J.; Mondragon-Ramirez, C.; Vorobyov, I.; Mackerell, A. D., Jr; Pastor, R. W. Update of the CHARMM All-Atom Additive Force Field for Lipids: Validation on Six Lipid Types. *J. Phys. Chem. B* **2010**, *114*, 7830–7843.

(8) Parrinello, M.; Rahman, A. Polymorphic Transitions in Single Crystals: a New Molecular Dynamics Method *Journal of Applied physics* **1981**.

(9) Nose, S.; Klein, M. L. Constant Pressure Molecular Dynamics for Molecular Systems *Mol. Phys.* **1983**.

(10) Darden, T.; York, D.; Pedersen, L. Particle Mesh Ewald: an NT Log(N) Method for Ewald Sums in Large Systems *J. Chem. Phys.* **1993**, *98*, 10089.

(11) Bussi, G.; Donadio, D.; Parrinello, M. Canonical Sampling Through Velocity Rescaling *J. Chem. Phys.* **2007**, *126*, 014101.

(12) Piggot, T. J.; Piñeiro, Á.; Khalid, S. Molecular Dynamics Simulations of Phosphatidylcholine Membranes: a Comparative Force Field Study *J. Chem. Theo. Comput.* **2012**, *8*, 4593–4609.

(13) Lupyan, D.; Mezei, M.; Logothetis, D. E.; Osman, R. A Molecular Dynamics Investigation of Lipid Bilayer Perturbation by PIP2. *Biophys. J.* **2010**, *98*, 240–247.

(14) Kooijman, E. E.; King, K. E.; Gangoda, M.; Gericke, A. Ionization Properties of Phosphatidylinositol Polyphosphates in Mixed Model Membranes *Biochemistry* **2009**, *48*, 9360–9371.